Substrate Gating of Contact Resistance in Graphene Transistors

Dionisis Berdebes, *Student Member, IEEE*, Tony Low, *Member, IEEE*, Yang Sui, *Member, IEEE*, Joerg Appenzeller, *Fellow, IEEE*, and Mark S. Lundstrom, *Fellow, IEEE*

***Abstract*—Metal contacts have been identified to be a key technological bottleneck for the realization of viable graphene electronics. Recently, it has been observed that for structures that possess both a top and a bottom gate, the electron–hole conductance asymmetry can be modulated by the bottom gate. In this paper, we explain this observation by postulating the presence of an effective thin interfacial dielectric layer between the metal contact and the underlying graphene. Electrical results from quantum transport calculations accounting for this modified electrostatics corroborate well with the experimentally measured contact resistances. This paper indicates that the engineering of a metal–graphene interface is a crucial step toward reducing the contact resistance for high-performance graphene transistors.**

***Index Terms*—Contacts, graphene transistor, Landauer, nonequilibrium Green's function (NEGF), quantum transport.**

I. Introduction

SINCE its experimental isolation [1]–[3], graphene has attracted significant attention from the scientific community due to its unique electronic structure and physical properties [4], [5]. Its excellent transport properties and the ability to tune the carrier concentration with electrical gates also make it a material with great technological promise. Potential applications range from radio-frequency (RF) devices and transistors [6]–[8] to biosensors [9] and flexible electronics [10]. The metal–graphene contact is, however, a key technological challenge for graphene-based electronic devices. For current-generation silicon metal–oxide–semiconductor field-effect transistors (MOSFETs), the International Technology Roadmap for Semiconductors calls for a resistance of 80 $\Omega \cdot \mu$m per contact, which is about 10% of the transistor's on-resistance V_{DD}/I_{ON} [11]. Graphene's excellent transport properties should produce transistor on-resistances considerably lower than those of silicon MOSFETs. To realize the performance potential afforded by the excellent transport properties of graphene, exceptionally low contact resistances will be required [6], [7]. It is, therefore, essential to develop a thorough understanding of metal–graphene contacts and of the fundamental lower limits for the contact resistance. In this paper, we develop a model that explains the recently observed substrate modulation of contact resistance in graphene transistors [12], [13]. We argue that this effect is due to the presence of an effective thin metal–graphene interfacial dielectric layer. Using this model, we estimate two important components of the series resistance and establish lower bounds for the contact resistance. This paper provides an improved understanding of the metal–graphene contact that may prove useful for improving device performance.

Graphene is sensitive to external perturbations due to its all-surface and zero-volume nature [9]. Charge transfer between metal and graphene due to a work-function difference dopes the underlying graphene [14]. Contacts, therefore, introduce a built-in electrostatic junction within graphene, which was experimentally observed using scanning tunneling microscopy [15]. A distinct experimental signature was the asymmetry of resistance in back-gated devices [16], [17]. The sign of this asymmetry reflects the doping of the graphene underneath the metal. Recently, devices with top and bottom gating schemes, as shown in Fig. 1, were experimentally realized [12], [13]. The measurement of resistance versus top-gate voltage V_T revealed an asymmetry, whose sign and magnitude were modulated by the back-gate voltage V_B. This observation strongly suggests that the graphene doping underneath the metal was substantially modulated by the back-gate voltage.

It is instructive to recall that in standard metal–semiconductor junction theory, the Schottky barrier height is given by the difference between the metal work function ϕ_M and the electron affinity χ_S of the semiconductor, when there is no Fermi-level pinning. However, the metal–graphene binding is comparatively weaker. The nature of the interfacial metal–graphene chemical bonding is still a subject of theoretical study [14], [18], [19]. In case of weak electronic interaction between metal and graphene (physisorption), graphene's pristine electronic band structure is preserved, and the metal–graphene interfacial layer demonstrates a dielectric-like behavior. This layer can then be modeled with interfacial capacitance C_M. If $C_M \gg C_B$ and $C_M \gg C_{\mathrm{qm}} \approx e^2 D(E_F - E_{D1})$, where D stands for the density of states, then one expects the Dirac point of graphene

Manuscript received April 18, 2011; revised June 23, 2011 and July 28, 2011; accepted July 29, 2011. Date of publication August 30, 2011; date of current version October 21, 2011. This work was supported in part by the Nanoelectronics Research Initiative through the Institute for Nanoelectronics Discovery and Exploration Center and in part by the Focus Center for Material Structures and Devices. The review of this paper was arranged by Editor H. Jaouen.

D. Berdebes, J. Appenzeller, and M. S. Lundstrom are with the Network for Computational Nanotechnology, Birck Nanotechnology Center, School of Electrical and Computer Engineering, Purdue University, West Lafayette, IN 47906 USA (e-mail: dionisis@purdue.edu).

T. Low is with the IBM T.J. Watson Research Center, Yorktown Heights, NY 10598 USA.

Y. Sui is with the GE Global Research Center, Niskayuna, NY 12309 USA.

Color versions of one or more of the figures in this paper are available online at http://ieeexplore.ieee.org.

Digital Object Identifier 10.1109/TED.2011.2163800

0018-9383/$26.00 © 2011 IEEE

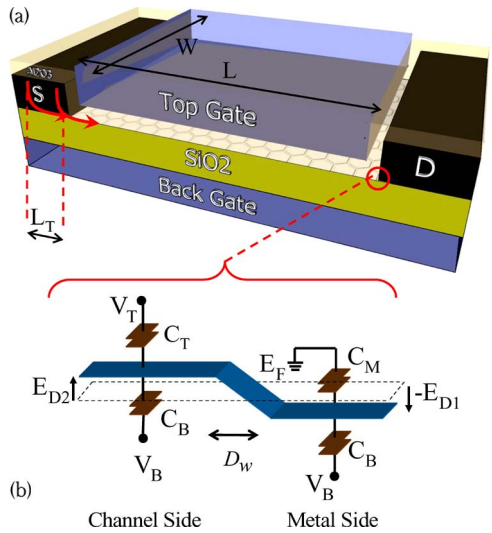

Fig. 1. (a) Fully top/bottom-gated graphene structure and (b) modeled potential profile across metal-coated and channel parts of the graphene sheet. With $C_T/(C_B)$ we denote the top/(bottom) gate capacitance values, whereas C_M accounts for the interfacial capacitance between metal and graphene. The positive/(negative) sign of the difference $E_F - E_D$ between the Fermi level E_F and the Dirac surface E_D accounts for n/(p) doping of the respective region.

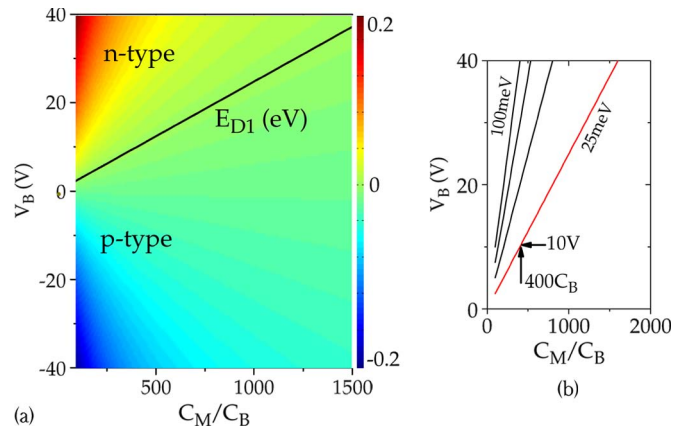

Fig. 2. (a) Surface potential (left) and (b) modulation of the neutrality condition (right) of the metal-coated side of graphene. The doping of the metal-coated side of graphene is modulated with the back gate V_B and depends also on the value of the interfacial capacitance C_M and the work-function difference $\delta\phi$. The crossing line(s) in both figures reflect(s) zero-surface potential (Dirac lines). In the inset (right), the modulation of the neutrality condition of the metal-coated side of graphene is applied, in direct correspondence to the equation $C_M\delta\phi - C_B V_B = 0$.

E_{D1} to be stationary with respect to ϕ_M. The above limit describes the standard metal–semiconductor junction since C_M is generally significantly larger than the semiconductor capacitance. If $C_M \leq C_{\rm qm}$, it is possible to modulate E_{D1} with applied voltage V_B. Consideration of this fact is key to explaining the experimental results [12] of the device shown in Fig. 1.

II. Model

From Gauss's law, the electrostatic equations governing the graphene underneath the contact (region 1) and the top gate (region 2) are

$$C_M(E_{D1} + \delta\phi) + C_B(E_{D1} - eV_B) = e^2 n_1 \quad (1)$$

$$C_T(E_{D2} - eV_T) + C_B(E_{D2} - eV_B) = e^2 n_2 \quad (2)$$

where $\delta\phi \equiv \phi_M - \phi_G$ is the work-function difference between metal and graphene, $en_i = E_{Di}^2/\pi(\hbar v_f)^2$, and no Fermi-level pinning is considered. Note that E_F is taken to be zero as reference. The transition between regions 1 and 2 is described by an analytical screening model [20], assuming a linear-graded junction with width D_w. Junction resistance $\mathcal{R}_{\rm junc}$ is then quantum mechanically computed using a previously developed mode-space nonequilibrium Green's function (NEGF) method for graphene [21].[1] For our ballistic study, the effect of temperature impacts our results only through the thermal smearing due to Fermi–Dirac distribution function, which is included in this paper.

In the experiment [12], the gate capacitance values are known, i.e., $C_B \approx 1.15 \times 10^{-4} Fm^{-2}$ and $C_T = 42C_B$. On the other hand, C_M is a quantity to be determined. Ti/Pd/Au is used for the metal contacts. For our calculations, we assumed that $\delta\phi \approx 25$ meV, a value that is sensible for our experimental metal stack.[2] Fig. 2(a) plots E_{D1} as a function of V_B and C_M. As expected, V_B modulates the doping in region 1 with greater ease when C_M is smaller. In the experiments, it was observed that the conductance as a function of V_T exhibits the least asymmetry when $V_B \approx 10$ V [see Fig. 3(a)]. This suggests that when $V_B \approx 10$ V, $E_{D1} \approx 0$ (the charge neutrality point), which then also allows us to pin down C_M to be $C_M \approx 400C_B$. On the other hand, a different choice of $\delta\phi$ would correspondingly yield a different C_M, as illustrated in Fig. 2(b).

III. Results

The measured conductance $G(V_T)$ for different values of V_B is shown in Fig. 3(a). The observed asymmetry in $G(V_T)$ changes sign at about $V_B = 10$ V. To facilitate the comparison between the experiment and a ballistic theory, we extract the odd component of the resistance [22] from the experiment, which is given by $\mathcal{R}_{\rm odd} \equiv 1/2[\mathcal{R}(\delta V_T) - \mathcal{R}(-\delta V_T)]$, where δV_T is V_T with respect to the Dirac point voltage. The quantity $\mathcal{R}_{\rm odd}$ then allows for a quantitative comparison between the experimentally measured $G(V_T)$ and the numerically

[1] In the work of L. M. Zhang and M. M. Fogler [20], the calculated analytical screening model for the transition region was used for the extraction of values for $\mathcal{R}_{\rm junc}$, based on previously reported transfer matrix formalism [39]. In the current model, the employment of that analytical screening model for the transition region allowed for an NEGF calculation of $\mathcal{R}_{\rm junc}$, which accounted for gating [21].

[2] Literature on metal work function on graphene reports a wide range of $\delta\phi$, suggesting that experimental condition and surface physics introduce variability. Experiments have provided indication about the metal–graphene function difference, based on a quantitative $R_{\rm ODD}$ analysis [16], and a photocurrent study [37]. From a computational standpoint, density functional theory (DFT) studies [14], [18] have provided support for a spectrum of work-function differences in a range $\delta\phi = [-0.3, 0.5]$ eV for several different metal compositions.

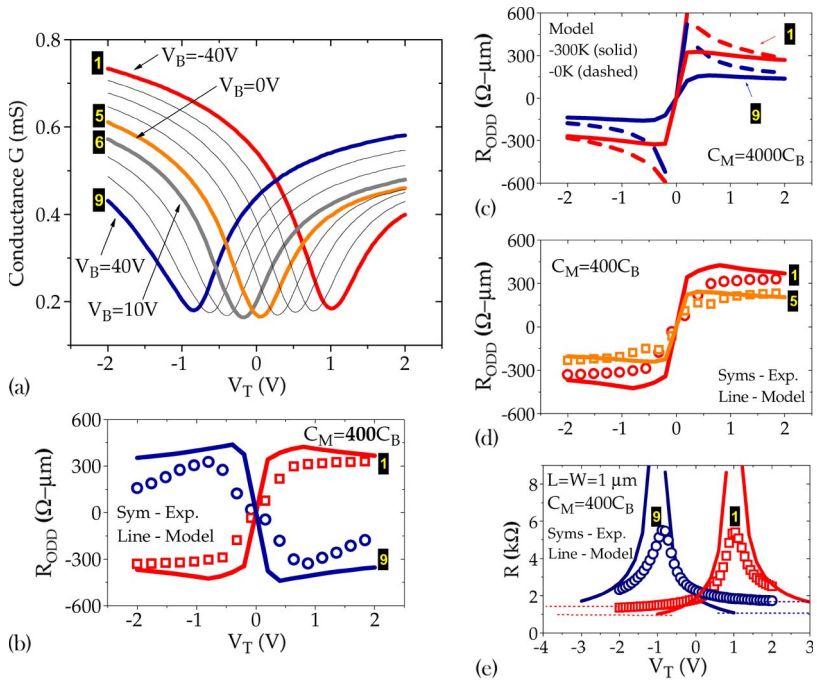

Fig. 3. Study of the conductance asymmetry of the Chen/Appenzeller experiments [12]. (a) Experimental G–V_T curves for different back-gate voltages V_B, ranging from $V_B = -40$ V to $V_B = 40$ V. (b) Comparison of model prediction versus experiment for the odd part of resistance $\mathcal{R}_{\rm odd}$ versus top-gate voltage V_T for $V_B = -40$ V and $V_B = 40$ V, assuming an interfacial capacitance $C_M = 400C_B$ and a temperature of $T = 300$ K. (c) Model prediction of $\mathcal{R}_{\rm odd}$ for the same voltages for an elevated interfacial capacitance $C_M = 4000C_B$, for (solid line) $T = 300$ K and (dashed line) $T = 0$ K. (d) Odd part of resistance ($\mathcal{R}_{\rm odd}$) versus V_T for $V_B = 0$ V and $V_B = -40$ V with $C_M = 400C_B$ at $T = 300$ K. (e) Experimental R–V_T curves for $V_B = -40$ V and $V_B = 40$ V versus our NEGF model, assuming an interfacial capacitance $C_M = 400C_B$, a work-function difference $\delta\phi = 0.025$ eV, and a temperature of $T = 300$ K.

calculated $\mathcal{R}_{\rm junc}(V_T)$. Although interface charge, moisture, and chemicals in the vicinity may impact the transport properties of the graphene devices, these effects can be minimized by careful control of the fabrication process and the measurement conditions so that any asymmetry can be entirely attributed to the graphene p-n junction.

In Fig. 3(b), the striking experimental observation of asymmetry inversion, as it is observed in $\mathcal{R}_{\rm odd}$ versus $V_B = -40$ V and $V_B = 40$ V, is compared with our modeled $\mathcal{R}_{\rm odd}$ for a work-function difference $\delta\phi = 0.025$ eV and interfacial capacitance $C_M = 400C_B$. As previously elucidated, modulation of the doping of graphene underneath the metal is possible because C_M is not large enough to completely dominate over $C_{\rm qm}$. In fact, for a moderate carrier concentration of 1×10^{12} cm^{-2}, one obtains $C_{\rm qm} \approx 0.75C_M$. If one assumes that the metal–graphene interfacial layer is an air gap, $C_M = 400C_B$ would then translate to a physical thickness of only 2 Å. This is in good agreement with recent density functional studies [23], with a predicted metal–graphene binding distance of ≈3.5 Å. The possibility of sign inversion is, however, conditional. For example, if we use a value of $C_M = 4000C_M$ instead of $C_M = 400C_B$, sign inversion of $\mathcal{R}_{\rm odd}$ would not be observed within the V_B range of interest, as shown in Fig. 3(c). In Fig. 3(d), we show that the increasing odd resistance with increasing $|V_B|$, as it is observed in the experiment for $V_B = 0$, -40 V, can be also captured with our simulation using $C_M = 400C_B$.

Up until now, we only considered $\mathcal{R}_{\rm junc}$ and its contribution to the asymmetric part of the contact resistance. Previous studies [24], [25] of the intrinsic transport properties of graphene on substrate allow one to make reasonable estimates of the channel resistance $\mathcal{R}_{\rm cha}$ by including contributions due to acoustic/optical phonons and substrate-induced remote phonons. However, their contributions relative to $\mathcal{R}_{\rm junc}$ are not as significant.[3] The modest mobility of ≈500 cm^2/Vs was extracted from the experiment in vicinity of the Dirac point, suggesting high levels of impurities [26]. Here, we model the impurity-limited resistivity with the Landauer formula using a mean free path proportional in energy, i.e., $\rho_{\rm im}^{-1} = h/2e^2 \times M^{-1}[L^{-1} + (\alpha E)^{-1}]$, where α is used to fit the mobility, and M is the number of modes normalized to W. In Fig. 3(e), we compare the experimental resistance with the calculated sum $\mathcal{R}_c = \mathcal{R}_{\rm cha} + \mathcal{R}_{\rm junc}$. By construction, our model does not capture the physics at the Dirac point. However, far away from the Dirac point, one observes an unaccounted excess resistance in the experiment of ≈500 Ω, the origin of which is the subject of the subsequent discussion.

Other contributions to contact resistance include the current crowding effects due to access geometry and the presence of the metal–graphene interfacial layer. The latter implies that current has to tunnel across a dielectric layer, encapsulated in the electrical quantity $C_M = 400C_B$. The tunneling resistivity $\rho_{\rm tun}$ can be estimated using a model for quasi-bound electrons [27], commonly used in the study of gate leakage current in semiconductor inversion layers [28]. It is given by $\rho_{\rm tun} = P\tau/e^2D$, where P is the Wentzel–Kramers–Brillouin tunneling

[3]For example, acoustic phonons limited resistivity is only 30 Ω at room temperature [24]. Since our device has an aspect ratio of $W/L = 1$. This contribution is not significant compared to $\mathcal{R}_{\rm junc}$.

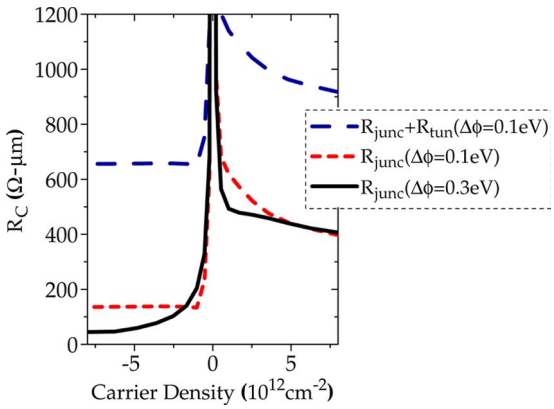

Fig. 4. Estimates of various components of contact resistance in graphene transistors. With the long-dashed line, we denote our modeled ballistic prediction for the junction resistance plus the tunneling resistance $\mathcal{R}_c = \mathcal{R}_{\rm junc} + \mathcal{R}_{\rm tun}$ for a pair of interfaces. After subtraction of $\mathcal{R}_{\rm tun}$, we get the ballistic result for the lower bound of the (short-dashed line) contact resistance $\mathcal{R}_{\rm junc}$, assuming a work-function difference $\phi_M - \phi_G = 0.1$ eV. Last, an increase in the work-function difference to $\phi_M - \phi_G = 0.3$ eV further reduces our ballistic prediction for the junction resistance (solid line) $\mathcal{R}_{\rm junc}$. (The region near $n_s = 0$ should be disregarded since it is strongly affected by spatial potential fluctuations, which are not considered in our model.)

probability estimated to be ≈0.3, and τ is known as the classical bounce time [27], which in graphene is simply $\tau = 2t_g/v_f$, with t_g and v_f being the thickness of graphene and Fermi velocity, respectively. Here, we take t_g to be the carbon–carbon bond length, i.e., 1.44 Å. This yields us a tunneling resistance estimate of $\rho_{\rm tun} \approx 5.2 \times 10^{-6}\ \Omega \cdot {\rm cm}^2$ for a pair of contacts. This value is reasonably close to a recently reported [29] experimental value of $\approx 5 \times 10^{-6}\ \Omega \cdot {\rm cm}^2$.

Expanding the prior analysis to the spatial distribution of carrier flow, the current crowding effects due to the metal–graphene access geometry lead to an effective electrical area for the contact where current flows, given simply by $W \times L_T$, where $L_T = \sqrt{\rho_c/\rho_g}$ is commonly known as the transfer length. With ρ_c and ρ_g, we denote the specific contact resistivity and the sheet resistance of the graphene layer underneath, respectively. Using our estimated $\rho_{\rm tun} \approx 5.2 \times 10^{-6}\ \Omega \cdot {\rm cm}^2$ and a sheet resistance $\rho_g = 1660\ \Omega\ \square$ from the experiment [12], at a channel carrier concentration $n_s \approx 5 \times 10^{12}\ {\rm cm}^{-2}$, we find $L_T \approx 560$ nm. Given the experiment-to-experiment variations in ρ_c and ρ_g, this value is within a reasonable range [29].

IV. Conclusion

Recently reported contact resistance values lie in the range $\mathcal{R}_c \approx 600 - 10^4\ \Omega \cdot \mu$m [13], [29]–[33] (see Appendix D). These values are considerably above what is required for high-performance transistors [11]. Here, we examine several issues related to the fundamental limit to $\mathcal{R}_c$.

In Fig. 4, we consider the contact resistance for a pair of interfaces $\mathcal{R}_c$, incorporating both the tunneling component $\mathcal{R}_{\rm tun} = 520\ \Omega$ that we extracted previously and the junction component $\mathcal{R}_{\rm junc}$ assuming a work-function difference $\phi_M - \phi_G = 0.1$ eV (long-dashed line). It is expected that $\mathcal{R}_{\rm tun}$ can considerably vary from experiment to experiment due to different contact materials, interface conditions, etc. [13], [29]–[34]. Significant reductions in $\mathcal{R}_{\rm tun}$ will be crucial, and the contact metal and deposition and annealing conditions will be critical factors. Recently, it has been demonstrated that a low-power plasma O_2 treatment prior to metal deposition is beneficial in improving $\mathcal{R}_{\rm tun}$ [35]. Another very recent study has demonstrated that $\mathcal{R}_{\rm tun}$ is temperature dependent, possibly due to an expansion of graphene–metal distance [34].

The ballistic junction component $\mathcal{R}_{\rm junc}$, on the other hand, seems to have a more universal nature since it is limited by the electrostatics condition and the number of conducting channels bottleneck [21]. To illustrate this, we plotted $\mathcal{R}_{\rm junc}$ for $\phi_M - \phi_G = 0.1$ eV and 0.3 eV in Fig. 4. For channel carrier concentration $n_s < 0$, a lower resistance plateau forms. The resistance value of this plateau is described by the quantum contact resistance $R_Q = h/2e^2 \times M^{-1}W$ [36], where M is the number of current-carrying modes, and this limit is imposed by $\Delta\phi$ at the metal side of the junction. Indeed, for $\Delta\phi = 0.1$ eV (short-dashed line), one finds $R_Q \approx 134\ \Omega \cdot \mu$m, whereas for $\Delta\phi = 0.3$ eV (solid line), one finds $R_Q \approx 45\ \Omega \cdot \mu$m. In the latter case, however, for moderate negative values of n_s, where the plateau has not been reached, quantum resistance R_Q is limited by the number of modes in the channel, and $R_Q = h/2e^2 \times 1/2\sqrt{\pi/n_s}$ holds valid instead. The elevated right branch, when $n_s > 0$, is due to the effect of interband tunneling. Selection of appropriate metal work function or approaches to engineer sharp p-n junction, i.e., chemical doping [6], are promising directions.

In conclusion, we have proposed a model that explains the gate-dependent resistance asymmetry observed in experiments and provides increased understanding of the different components of the contact resistance in graphene transistors. We have shown that the existence of an interfacial layer between metal and graphene can explain the back gating of the contacts observed by Chen and Appenzeller [12]. The importance of such an interfacial layer to devices was also pointed out in two very recent studies. Robinson *et al.* showed that residual photoresist following lithography can lead to high contact resistance [35], and Xia *et al.* explained the temperature dependence of the contact resistance in terms of the graphene to metal distance [34].[4] This paper and these studies point to the need for further understanding of the metal–graphene interfacial layer as a prerequisite for engineering a good contact resistance for graphene electronics.

Appendix A
Quantum Ballistic Transport

In this paper, the simulation methods that are used closely follow the ones that were employed in previous work [21], i.e., ballistic NEGF method. Thus, we constrain ourselves to a brief

[4]In the work of Xia *et al.* [34], a Landauer model is employed to interpret temperature-dependent graphene contact resistance data, which involves tunneling probability through the metal–graphene interface $T_{\rm MG}$ and tunneling probability over the graphene junction barrier T_k. The two probabilities are cascaded in a coherent manner. In this paper, on the other hand, the two probabilities are separated to yield independent resistance components $\mathcal{R}_c = \mathcal{R}_{\rm tun} + \mathcal{R}_{\rm junc}$.

description of the main features. Central to our calculations is the Green's function

$$G(\epsilon, k_y) = [(\epsilon + i\delta)I - H(k_y) - U - \Sigma_l(\epsilon, k_y) - \Sigma_s(\epsilon, k_y)]^{-1} \tag{3}$$

where ϵ is the Fermi energy, δ is the broadening term, U is electrostatic potential, and Σ_s is the contact self-energy. The Hamiltonian H has a tridiagonal form

$$H = \begin{pmatrix} \alpha & \beta_1 & \vdots \\ \beta_1^\dagger & \alpha & \beta_2 \\ \vdots & \beta_2^\dagger & \alpha \end{pmatrix} \tag{4}$$

where α, β_1, and β_2 are respectively

$$\alpha = \begin{bmatrix} 0 & t_c \\ t_c & 0 \end{bmatrix}, \quad \beta_1 = \begin{bmatrix} 0 & 0 \\ t_y^* & 0 \end{bmatrix}, \quad \beta_2 = \begin{bmatrix} 0 & 0 \\ t_y & 0 \end{bmatrix} \tag{5}$$

and $t_y = t_c + t_c e^{ik_y a_0}$, where t_c denotes the nearest neighbor coupling energy in a tight binding model, and $a_0 = \sqrt{3}a_{\rm cc}$ is the lattice parameter, where $a_{\rm cc}$ is the carbon–carbon distance.

The contacts' self-energy values $\Sigma_{l,r}(\epsilon, k_y)$ are calculated with the use of $\Sigma_{l,r}(\epsilon, k_y) = \tau_i g_i \tau_i^\dagger$, where g_i is the surface Green's function associated with the contacts. For the transverse momentum k_y, the values are quantized according to the box boundary condition by Brey and Fertig [38]. Lastly, the charge current, assuming coherent transport and summing over transverse modes, is

$$I_i(\epsilon) = 2q/h \sum_{k_y} \text{trace}\left[\Sigma_i^{in}(\epsilon)A(\epsilon) - \Gamma_i(\epsilon)G_n(\epsilon)\right] \tag{6}$$

where $A(\epsilon) = i(G - G^\dagger)$ is the local density of states, $\Sigma_i^{\rm in}(\epsilon) = f_0(\epsilon)\Gamma_i(\epsilon)$ is the filling function, $f_0(\epsilon)$ is the equilibrium Fermi function at the contact regions, and $\Gamma_i(\epsilon) = i(\Sigma_i - \Sigma_i^\dagger)$ is the contact broadening factor. The electron correlation function $G_n(\epsilon)$ is defined as $G_n(\epsilon) = G(\Sigma_l^{\rm in}(\epsilon) + \Sigma_r^{\rm in}(\epsilon))G^\dagger$.

Appendix B
Quantum Capacitance

From the electrostatic equations in the main paper, i.e., (1) and (2), we can compute n_1 as a function of applied V_T. Total capacitance $C_{\rm Total}$ is then numerically computed from $C_{\rm Total} = d(en_1)/dV_T$. The quantum capacitance can then be obtained from $C'_{\rm QM} = [C_{\rm Total}^{-1} - C_M^{-1}]^{-1}$. In the literature, one often uses the approximate expression for quantum capacitance $C_{\rm QM} \approx e^2 D$, where $D = 2V_T/(\pi\hbar^2 v_f^2)$ is the density of states. In Fig. 5, we plot various capacitance values, i.e., $C_{\rm Total}$, C_M, $C'_{\rm QM}$, and $C_{\rm QM}$ in the graphene region underneath the metal contact. As observed, the quantum capacitance of graphene exceeds the interfacial capacitance C_M at moderate carrier concentration of $\approx 3 \times 10^{12}$ cm^{-2}.

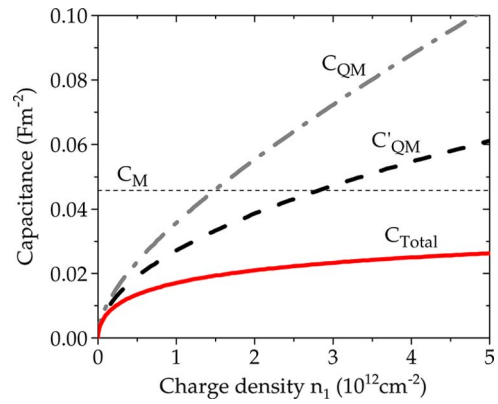

Fig. 5. Plot of various capacitance values as a function of n_1 in the graphene region underneath the metal contact. We assumed parameters from the main paper, i.e., $C_B = 1.15 \times 10^{-4} Fm^{-2}$ and $C_T = 42C_B$.

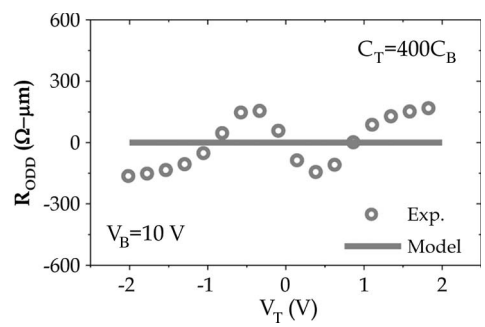

Fig. 6. Plot of experimental $R_{\rm ODD}$ for a back-gate voltage of $V_B = 10$ V versus the explicit model condition of zero $R_{\rm ODD}$ for the same voltage.

Appendix C
On the Extraction of Work-Function Difference and Interfacial Capacitance

For the analysis of the Chen/Appenzeller experiment, the identification of several parameters is essential. In particular, one has to identify the interfacial metal–graphene capacitance C_M, the top-channel capacitance C_T, and the work-function difference $\delta\phi$. For the determination of the top-gate capacitance, one can use the charge neutrality condition for the channel $C_M V_T + C_B V_B = 0$ to extract a value of $C_T = 42C_B$, where for the back-gate capacitance, we have $C_B \approx 1.14 \times 10^{-4}$ F since the substrate is made of 300-nm SiO_2 dielectric. Since the top-gate Al_2O_3 dielectric thickness is known to be 10 nm, this would translate to a top-gate dielectric constant of 5.42, which is less than the typical bulk value of 9.34. The values of C_M and $\delta\phi$ can be extracted in a similar fashion, but not independently. When the metal region is biased at the Dirac point, it satisfies the condition $C_M\delta\phi + C_B V_B = 0$. Arguably, this condition corresponds to the experimental transfer curve with the minimum asymmetry, i.e., $V_B \approx 10$ V, as shown in Fig. 6. At this back-gate voltage, we can extract a set of values for $\{C_M, \delta\phi\}$ that satisfies the above condition, i.e., $C_M\delta\phi + C_B 10\ \text{V} = 0$. Within this locus, the parameter set $\{C_M, \delta\phi\} = \{400C_B, 0.05\ \text{eV}\}$ is a reasonable choice for this paper.

In this paper, the metal contacts employed are made of Ti/Pd/Au. For our calculations, we choose a value of $\delta\phi = 0.025$ eV, a value that could be sensible for this particular

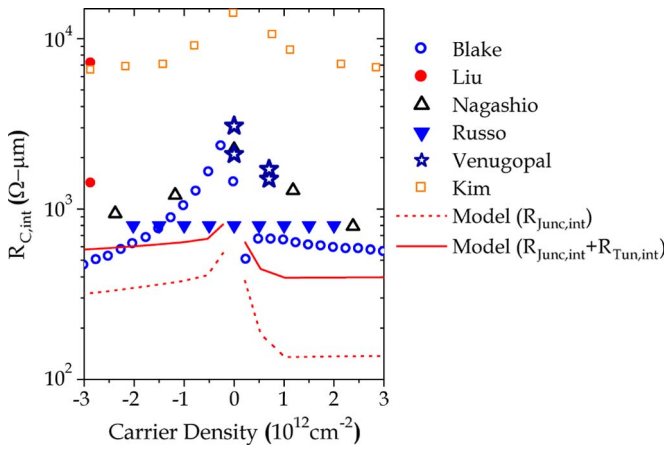

Fig. 7. Compilation of reported experimental values for graphene contact resistance per interface versus our (dashed line) modeled metal–graphene junction resistance $\mathcal{R}_{\mathrm{junc,int}}$, and our (solid line) modeled metal–graphene junction resistance plus the tunneling resistance $\mathcal{R}_{c,\mathrm{int}} = \mathcal{R}_{\mathrm{junc,int}} + \mathcal{R}_{\mathrm{tun,int}}$. The elevated values of our model for the left branch come as a result of a graphene p-n junction formation for a work-function difference $\phi_M - \phi_G = -0.1$ eV.

metal stack. Although higher values of $\delta\phi$ are also possible, this would translate to a smaller value of C_M in order to satisfy the condition of $C_M\delta\phi + C_B V_B = 0$ for $V_B = 10$ V. Smaller values of C_M would also inevitably lead to a larger dielectric thickness, thereby suppressing the amount of current flow through the graphene device. If we assume that the metal–graphene interfacial capacitance is due to an air gap, our assumed value of $C_M = 400C_B$ translates to a physical thickness of only 0.2 nm, assuming the dielectric constant of air. The extracted metal–graphene gap comes in good agreement with what has been reported in several DFT interface studies. As it was reported in this paper, this gap also yields a tunneling resistance value that is compatible with what has been experimentally measured. In addition to all the previous arguments, the parametric set $\{C_M, \delta\phi\} = \{400C_B, 0.05\text{ eV}\}$ allowed us to reasonably fit the modulation of the resistance asymmetry R_{ODD}.

Appendix D
Compilation of Measured Contact Resistances Versus Our Model

Here, we shall put into perspective our model, for $\mathcal{R}_{c,\mathrm{int}} = \mathcal{R}_{\mathrm{junc,int}} + \mathcal{R}_{\mathrm{tun,int}}$, with the reported values of contact resistance per interface ($\mathcal{R}_{c,\mathrm{int}}$) extracted in the literature [13], [29]–[33], as shown in Fig. 7. A wide range of reported values for $\mathcal{R}_{c,\mathrm{int}}$ is observed partly due to different experimental conditions, materials, device structures, and extraction methods. The various extraction methods include the standard transmission line measurement [29], [31], [32], saturation resistance at high-back-gate bias [33], and subtraction from four-probe measurement [30].

The general observation of the variance and the uncertainty of the extracted contact resistance values in the literature could be a pointer to the importance of the tunneling resistance, which heavily depends on the fabrication process and considerably varies from experiment to experiment. Our ballistic calculation though, for the junction resistance $\mathcal{R}_{\mathrm{junc,int}}$, seems to have a more universal nature, as it was discussed in the main body of this paper. Having plotted $\mathcal{R}_{\mathrm{junc,int}}$ with a work-function difference $\phi_M - \phi_G = -0.1$ eV, we observe that the junction resistance falls below all measured values, even if we tune the work-function difference of our model within a reasonable window.[5] If we now add the $\mathcal{R}_{\mathrm{tun,int}}$ term that we extracted for the Chen/Appenzeller experiments [12] to $\mathcal{R}_{\mathrm{junc,int}}$, we get a number for the contact resistance that is closer to the range of most measured data [12]. The largest values of $\mathcal{R}_{c,\mathrm{int}}$ in Fig. 7 were observed when the device has a fraction of the channel uncovered by the top gate [13].

Acknowledgment

The authors would like to thank the Network for Computational Nanotechnology for providing computational support.

References

[1] K. S. Novoselov, A. K. Geim, S. V. Morozov, D. Jiang, Y. Zhang, S. V. Dubonos, I. V. Grigorieva, and A. A. Firsov, "Electric field effect in atomically thin carbon films," *Science*, vol. 306, no. 5696, pp. 666–669, Oct. 2004.
[2] K. S. Novoselov, A. K. Geim, S. V. Morozov, D. J. M. I. Katsnelson, I. V. Grigorieva, S. Dubonos, and A. A. Firsov, "Two-dimensional gas of massless Dirac fermions in graphene," *Nature*, vol. 438, no. 7065, pp. 197–200, Nov. 2005.
[3] Y. B. Zhang, Y. W. Tan, H. L. Stormer, and P. Kim, "Experimental observation of the quantum hall effect and Berry's phase in graphene," *Nature*, vol. 438, no. 7065, pp. 201–204, Nov. 2005.
[4] A. K. Geim and K. S. Novoselov, "The rise of graphene," *Nat. Mater.*, vol. 6, no. 3, pp. 183–191, Mar. 2007.
[5] A. H. C. Neto, F. Guinea, N. M. R. Peres, K. S. Novoselov, and A. K. Geim, "The electronic properties of graphene," *Rev. Mod. Phys.*, vol. 81, no. 1, pp. 109–162, Jan. 2009.
[6] P. Avouris, "Graphene: Electronic and photonic properties and devices," *Nano Lett.*, vol. 10, no. 11, pp. 4285–4294, Sep. 2010.
[7] F. Schwierz, "Graphene transistors," *Nat. Nanotechnol.*, vol. 5, no. 7, pp. 487–496, Jul. 2010.
[8] Y. M. Lin, C. Dimitrakopoulos, K. A. Jenkins, D. B. Farmer, H. Y. Chiu, A. Grill, and P. Avouris, "100 ghz transistors from wafer scale epitaxial graphene," *Science*, vol. 327, no. 5966, p. 662, Feb. 2010.
[9] F. Schedin, A. K. Geim, S. V. Morozov, E. W. Hill, P. Blake, M. I. Katsnelson, and K. S. Novoselov, "Detection of individual gas molecules adsorbed on graphene," *Nat. Mater.*, vol. 6, no. 9, pp. 652–655, Sep. 2007.
[10] K. S. Kim, Y. Zhao, H. Jang, S. Y. Lee, J. M. Kim, K. S. Kim, J.-H. Ahn, P. Kim, J.-Y. Cho, and B. H. Hong, "Large scale pattern growth of graphene films for stretchable transparent electrodes," *Nature*, vol. 457, no. 7230, pp. 706–710, Feb. 2009.
[11] The National Technology Roadmap for Semiconductors, Semiconductor Industry Association, 2010.
[12] Z. Chen and J. Appenzeller, "Gate modulation of graphene contacts on the scaling of graphene fets," in *VLSI Symp. Tech. Dig.*, 2009, pp. 128–129.
[13] S. Kim, J. Nah, D. S. I. Jo, L. Colombo, Z. Yao, E. Tutoc, and S. K. Banerjee, "Realization of a high mobility dual-gated graphene field-effect transistor with Al_2O_3 dielectric," *Appl. Phys. Lett.*, vol. 94, no. 6, pp. 062107-1–062107-3, Feb. 2009.
[14] G. Giovannetti, P. A. Khomyakov, G. Brocks, V. M. Karpan, J. van den Brink, and P. J. Kelly, "Doping graphene with metal contacts," *Phys. Rev. Lett.*, vol. 101, no. 2, p. 026803, Jul. 2008.
[15] Y. Yu, Y. Zhao, S. Ryu, L. Brus, K. Kim, and P. Kim, "Tuning the graphene work function by electric field effect," *Nano Lett.*, vol. 9, no. 10, pp. 3430–3434, Oct. 2009.

[5] The particular value that we chose for $\delta\phi$ was motivated by Blake *et al.* [30]. In that study, the contact material was Ti, which yielded n-doped graphene and an elevated left branch.

[16] B. Huard, N. Stander, and D. Goldhaber-Gordon, "Evidence of the role of contacts on the observed electron–hole asymmetry in graphene," *Phys. Rev. B*, vol. 78, no. 12, p. 121402, Sep. 2008.
[17] J. Cayssol, B. Huard, and D. Goldhaber-Gordon, "Contact resistance and shot noise in graphene transistors," *Rhys. Rev. B*, vol. 79, no. 7, p. 075428, Feb. 2009.
[18] M. Vanin, J. J. Mortensen, A. K. Kelkkanen, J. M. Garcia-Lastra, K. S. Thygesen, and K. W. Jacobsen, "Graphene on metals: A van der waals density functional study," *Phys. Rev. Lett.*, vol. 81, no. 8, p. 081408, Feb. 2010.
[19] C. Gong, G. Lee, B. Shan, E. M. Vogel, R. M. Wallace, and K. Cho, "First principles study of metal–graphene interfaces," *J. Appl. Phys.*, vol. 108, no. 12, pp. 123711-1–123711-8, Dec. 2010.
[20] L. M. Zhang and M. M. Fogler, "Nonlinear screening and ballistic transport in a graphene p-n junction," *Phys. Rev. Lett.*, vol. 100, no. 11, p. 116804, Mar. 2008.
[21] T. Low, S. Hong, J. Appenzeller, S. Datta, and M. S. Lundstrom, "Conductance asymmetry of graphene p-n junction," *IEEE Trans. Electron. Devices*, vol. 56, no. 6, pp. 1292–1299, Jun. 2009.
[22] B. Huard, J. A. Sulpizio, N. Stander, K. Todd, B. Yang, and D. Goldhaber-Gordon, "Transport measurements across a tunable potential barrier in graphene," *Phys. Rev. Lett.*, vol. 98, no. 23, pp. 236803-1–236803-4, Jun. 2007.
[23] D. W. Boukhvalov, M. I. Katsnelson, and A. I. Lichtenstein, "Hydrogen on graphene: Electronic structure, total energy, structural distortions and magnetism from first-principles calculations," *Phys. Rev. B*, vol. 77, no. 3, p. 035427, Jan. 2008.
[24] J. Chen, C. Hang, S. Xiao, M. Ishigami, and M. Fuhrer, "Intrinsic and extrinsic performance limitations of grapheme devices on SiO_2," *Nat. Nanotechnol.*, vol. 3, no. 4, pp. 206–209, Apr. 2008.
[25] V. Perebeinos and P. Avouris, "Inelastic scattering and current saturation in graphene," *Phys. Rev. B*, vol. 81, no. 19, pp. 195442-1–195442-8, May 2010.
[26] S. Adam, E. H. Hwang, V. M. Galitski, and S. D. Sarma, "A self-consistent theory for graphene transport," *Proc. Nat. Acad. Sci.*, vol. 104, no. 47, pp. 18392–18397, Nov. 2007.
[27] A. J. Leggett, "Macroscopic quantum systems and the quantum theory of measurement," *Progr. Theor. Phys. Suppl.*, vol. 69, pp. 80–100, 1980.
[28] Y. T. Hou, M. F. Li, Y. Jin, and W. H. Lai, "Direct tunneling hole currents through ultrathin gate oxides in metal–oxide–semiconductor devices," *J. Appl. Phys.*, vol. 91, no. 1, pp. 258–264, Jan. 2002.
[29] K. Nagashio, T. Nishimura, K. Kita, and A. Toriumi, "Contact resistivity and current flow path at metal/graphene contact," *Appl. Phys. Lett.*, vol. 97, no. 14, pp. 143514-1–143514-3, Oct. 2010.
[30] P. Blake, R. Yang, S. Morozov, F. Schedin, L. Ponomarenko, A. Zhukov, R. Nair, I. Grigorieva, K. Novoselov, and A. Geim, "Influence of metal contacts and charge inhomogeneity on transport properties of graphene near the neutrality point," *Solid State Commun.*, vol. 149, no. 27/28, pp. 1068–1071, Jul. 2009.
[31] S. Russo, M. Craciun, M. Yamamoto, A. Morpurgo, and S. Tarucha, "Contact resistance in graphene-based devices," *Phys. E*, vol. 42, no. 4, pp. 677–679, Feb. 2010.
[32] A. Venugopal, C. Colombo, and E. M. Vogel, "Contact resistance in few and multilayer graphene devices," *Appl. Phys. Lett.*, vol. 96, no. 1, pp. 013512-1–013512-3, Jan. 2010.
[33] W. J. Liu, M. F. Li, S. H. Xu, Q. Zhang, Y. H. Zhu, K. L. Pey, H. L. Hu, Z. X. Shen, X. Zou, J. L. Wang, J. Wei, H. L. Zhu, and H. Y. Yu, "Understanding the contact characteristics in single or multilayer graphene devices," in *IEDM Tech. Dig.*, 2010, pp. 23.3.1–23.3.4.
[34] F. Xia, V. Perebeinos, Y. Lin, Y. Wu, and Ph. Avouris, "The origins and limits of metal–graphene junctrion resistance," *Nat. Nanotechnol.*, vol. 6, no. 3, pp. 179–184, Mar. 2011, DOI: 10.1038.
[35] J. A. Robinson, M. LaBella, M. Zhou, M. Hollander, R. Kasarda, Z. Hughes, K. Trumbull, R. Cavalero, and D. Snyder, "Contacting graphene," *Appl. Phys. Lett.*, vol. 98, no. 5, pp. 053103-1–053103-3, Jan. 2011.
[36] S. Datta, *Electronic Transport in Mesoscopic Systems*. Cambridge, U.K.: Cambridge Univ. Press, 1995.
[37] T. Mueller, F. Xia, M. Freitag, J. Tsang, and Ph. Avouris, "Role of contacts in graphene transistors: A scanning photocurrent study," *Phys. Rev. B*, vol. 79, no. 24, pp. 245430-1–245430-6, Jun. 2009.
[38] L. Brey and H. A. Fertig, "Electronic states of graphene nanoribbons studied with the Dirac equation," *Phys. Rev. B*, vol. 73, no. 23, p. 235411, Jun. 2006.
[39] V. V. Cheianov and V. I. Fal'ko, "Selective transmission of Dirac electrons and ballistic magnetoresistance of n-p junctions in graphene," *Phys. Rev. B*, vol. 74, no. 4, pp. 041403-1–041403-4, Jul. 2006.

Dionisis Berdebes (S'11) received the Dipl.-Ing. degree in electrical and computer engineering in 2008 from the University of Patras, Patras, Greece, and the M.S. degree in electrical engineering in 2010 from Purdue University, West Lafayette, IN, where he is currently working toward the Ph.D. degree in Mark Lundstrom Research Group, School of Electrical and Computer Engineering. His Diploma thesis involved 2-D simulation of photonic crystals, and his M.S. thesis focused on the analysis and characterization of graphene transistors.

His current research interests are in the theory, modeling, and simulation of solid-state devices with a focus on energy conversion.

Mr. Berdebes was a recipient of academic scholarships from the Greek/German states in 2007/2005 (IKY/DAAD).

Tony Low (M'08) received the Ph.D. degree from the National University of Singapore, Singapore, in 2008.

In 2007, he joined the Network for Computational Nanoelectronics, Purdue University, West Lafayette, IN, as a Visiting Scientist, and then, he became a Postdoctoral Associate in 2008. In 2011, he joined the Nanoscience Group of IBM T.J. Watson Research Center, Yorktown Heights, NY, and as the Liaison of the Institute for Nanoelectronics Exploration, which is a Nanoelectronics Research Initiative research center. His research interests are in the physical theory, modeling and simulation of materials and electronic transport phenomena. His work includes graphene, spintronics, and advanced Si, Ge, III–V transistors.

Dr. Low was a recipient of the IEEE Electron Devices Society Fellowship in 2005 and the Singapore Millennium Fellowship in 2006.

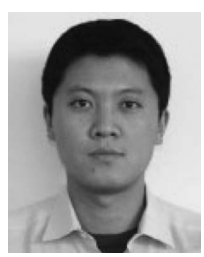

Yang Sui (S'04–M'07) was born in Harbin, China, in 1977. He received the B.S. degree in materials science and engineering from Tsinghua University, Beijing, China, in 2000, the M.S. degree in materials science and engineering from Iowa State University, Ames, in 2002, and the Ph.D. degree from Purdue University, West Lafayette, IN, in 2007. His Ph.D. thesis focused on design, simulation, fabrication, and characterization of high voltage SiC power switching devices.

He worked as a Postdoctoral Researcher on graphene nanoelectronics from 2007 to 2010 with the Birck Nanotechnology Center, Purdue University. He is currently a Research Staff Member with the GE Global Research Center, Niskayuna, NY.

Joerg Appenzeller (SM'04–F'10) received the M.S. and Ph.D. degrees in physics from the Technical University of Aachen, Aachen, Germany, in 1991 and 1995, respectively. His Ph.D. dissertation investigated quantum transport phenomena in low-dimensional systems based on III/V heterostructures.

He was a Research Scientist with the Research Center, Juelich, Germany, for one year before he became an Assistant Professor with the Technical University of Aachen in 1996. During his professorship, he explored mesoscopic electron transport in different materials, including carbon nanotubes and superconductor–semiconductor-hybrid devices. From 1998 to 1999, he was a Visiting Scientist with Massachusetts Institute of Technology, Cambridge, exploring the ultimate scaling limits of silicon metal–oxide–semiconductor field-effect transistor devices. From 2001 to 2007, he was a Research Staff Member with the IBM T. J. Watson Research Center, Yorktown, NY, where he was mainly involved in the investigation of the potential of carbon nanotubes and silicon nanowires for future nanoelectronics. Since 2007, he has been a Professor of electrical and computer engineering and a Scientific Director of Nanoelectronics in the Birck Nanotechnology Center, School of Electrical and Computer Engineering, Purdue University, West Lafayette, IN. His current research interests include novel devices based on low-dimensional nanomaterials such as nanowires, nanotubes, and graphene.

Mark S. Lundstrom (F'94) received the B.E.E. and M.S.E.E. degrees from the University of Minnesota, Minneapolis, in 1973 and 1974, respectively, and the Ph.D. degree in electrical engineering from Purdue University, West Lafayette, IN, in 1980.

From 1974 to 1977, he was with Hewlett-Packard Corporation, Loveland, CO, where he worked on integrated-circuit process development and manufacturing support. In 1980, he joined the School of Electrical Engineering, Purdue University, where he is currently the Don and Carol Scifres Distinguished Professor of Electrical and Computer Engineering. He was the Founding Director of the National Science Foundation-funded Network for Computational Nanotechnology, which created the nanoHUB.org science gateway. His current research interests center on the physics of small electronic devices, particularly nanoscale transistors, on carrier transport in semiconductor devices, and on devices for energy conversion, storage, and conservation.

Dr. Lundstrom is a member of the National Academy of Engineering and the recipient of several awards for his research and teaching.